Electrochimica Acta 140 (2014) 139–144

Contents lists available at ScienceDirect

Electrochimica Acta

journal homepage: www.elsevier.com/locate/electacta

Factors affecting the performance of the Zn-Ce redox flow battery

Georgios Nikiforidis, Rory Cartwright, David Hodgson [1], David Hall [2], Leonard Berlouis *

WestCHEM, Department of Pure and Applied Chemistry, University of Strathclyde, Glasgow G1 1XL, UK

ARTICLE INFO

Article history:
Received 12 December 2013
Received in revised form 24 April 2014
Accepted 25 April 2014
Available online 4 May 2014

Keywords:
Zn-Ce redox flow battery
Zinc electrodeposition
Hull cell

ABSTRACT

The Hull Cell was used to investigate the impact of current density j on the morphology and uniformity of zinc electrodeposited from a 2.5 mol dm^{-3} Zn^{2+} solution in 1.5 mol dm^{-3} methanesulfonic acid at 40 °C onto carbon-composite surfaces. The range of the applied deposition current density used was between 1 mA cm^{-2} and 100 mA cm^{-2}. Good, robust deposits were obtained when $j \geq 10$ mA cm^{-2} whereas at j's lower than this, patchy films formed due to the competing hydrogen evolution reaction (HER) on the bare carbon-composite surface. An understanding of these effects and its application in the redox flow battery enabled both the coulombic and cell potential efficiencies to be maintained at relatively high values, 90% and 69% respectively, indicating a successful inhibition of the HER on the fully formed Zn layer. Flow velocity at the low Reynolds number in the cell (Re <200) had little impact on the electrochemical cell performance. Depletion of the cerium species became an issue for long charge times.

1. Introduction

The development and implementation of robust, reliable and efficient energy storage systems in the 100's kW and MW scale has the potential to improve the stability of power systems and distribution networks (facilitating the load levelling). Furthermore, it can avoid the need of increasing generation capacity from greenhouse gas emitter systems and allow intermittent sources of energy generation such as wind, wave, tidal and solar to be brought into the play. Indeed, this rapidly growing demand of energy generated by renewable energy sources has given rise to increased market opportunities for electrical storage devices, such as redox flow batteries (RFBs).

Classical RFBs utilise a solution-based redox couple cycled through each half-cell to a reservoir, with a common strategy being to separate the half-cells by an ion exchange membrane in a bipolar plate filter-press reactor. Much of the early research on the redox flow batteries (RFBs) was carried out in the 1970s by Thaller and co-workers at the National Aeronautics and Space Administration (NASA) [1], the Energy Development Associates (EDA) [2], as well as several Japanese research institutions [3] on systems which included the Fe/Cr, Fe/Ti [4,5] and $Ru(bpy)_3/(BF_4)^2$ [6] couples. Skyllas-Kazacos *et al.* [7,8] worked on the all-vanadium RFB system during the 1980's and its success also led to the development of the vanadium-cerium [9], the vanadium-polyhalide [10,11], the vanadium-magnesium [12] and the vanadium-acetylacetonate [13] systems as these could provide higher cell potentials and energy densities. Since then, a variety of new RFBs have been developed, such as the soluble lead-acid [14,15], the cadmium-chloranil [16] and the bromine-polysulfide [17].

Hybrid RFBs differ from the classical RFBs in that they have a solution based redox couple as well as an electrode surface/solution electrode reaction (such as solid state transformation, gas evolution/reduction or metal deposition/stripping). Several hybrid flow batteries have also been examined, namely the copper-lead dioxide [18], zinc-bromine [19], zinc-cerium [20], zinc-nickel [21], zinc-chlorine [22] and zinc-air [23] batteries. It is not too surprising that the majority of these hybrid flow batteries are zinc-based as zinc has a relatively high negative reversible potential and is already extensively employed in the battery industry. Zinc/carbon primary batteries (Leclanché cells) were amongst the earliest batteries while zinc/air and nickel/zinc batteries have also found markets [24].

The zinc-cerium hybrid RFB has been under development since the early 1990's by Electrochemical Design Associates Inc. [25,26]. Further investigation of this system was conducted by Plurion Ltd., the University of Southampton [27–29] and the University of Strathclyde [30–33]. Its great advantage is its power to weight ratio due to its high open circuit cell voltage (E_{cell} = 2.4 V). This high cell potential (*c.f.* 1.4 V for the all-vanadium battery open circuit voltage) has naturally a direct impact on the amount of power that

* Corresponding author. Tel.: +44 141 548 4244; fax: +44 141 548 4822.
E-mail address: l.berlouis@strath.ac.uk (L. Berlouis).
[1] Electrochemical Innovation Lab, Department of Chemical Engineering, UCL, London WC1E 7JE, UK
[2] C-Tech Innovation Ltd, Capenhurst, Chester CH1 6EH, UK

http://dx.doi.org/10.1016/j.electacta.2014.04.150
0013-4686/

can be delivered at a specified current density. Methanesulfonic acid (MSA) is used as the supporting electrolyte as it allows the zinc and cerium electroactive species to dissolve at concentrations larger than 2.0 mol dm^{-3} and 8.0×10^{-1} mol dm^{-3}, respectively. The cerium salt used was cerium (III) carbonate and its solubility in MSA is about 10 times greater than in sulfuric acid [34,35].

Previous studies on the Zn-Ce flow cell have reported charge efficiencies of more than 90% and energy efficiencies above 60% at 10 mA cm^{-2} for over 100 cycles [30]. The material of choice there for the negative electrode was a polyvinyl ester or polyvinylidene fluoride-carbon composite material (BMA5) while a platinized titanium mesh was used as positive electrode. The electrolyte composition consisted of 5.9×10^{-1} mol dm^{-3} Ce(IV), 8.0×10^{-2} mol dm^{-3} Ce(III), 8.0×10^{-1} mol dm^{-3} Zn(II) and 3.5 mol dm^{-3} excess MSA. The anode and cathode compartments were separated by a Nafion® 117 membrane. Both electrodes had a geometric area of 100 cm^2. Leung *et al.* [27] reported coulombic, η_C and energy, η_ε efficiency values of 85% and 49% respectively under the application of ±50 mA cm^{-2} for a Zn-Ce RFB operating with similar electrolyte compositions. The charging time in this case was 15 minutes while the number of cycles was 57. Xie *et al.* [36] have reported an η_ε of 75% in a solution containing 5×10^{-1} mol dm^{-3} Ce(III) in 2.0 mol dm^{-3} MSA on the positive electrode and 5×10^{-1} mol dm^{-3} $ZnSO_4$ of aqueous solution on the negative electrode. However, a relatively small constant current of 200 mA was applied for 10 cycles. Furthermore, studies on a Zn-Ce undivided flow cell have been reported from Leung *et al.* [29]. The electrodes consisted of carbon felt compressed onto a planar carbon polyvinyl ester, while planar carbon polyvinyl was used as the negative electrode. The charge and energy efficiencies were 82% and 72% respectively, for a current density of 20 mA cm^{-2}. A detailed and up to date review on the latest developments on the zinc-cerium flow cell has been provided by Walsh *et al.* [37].

The Zn-Ce RFB cell in its simplest form consists of a single anode – cathode pair with a cation exchange membrane separating the electrodes. In the uncharged state, the zinc electrolyte and the cerium (III) electrolyte are stored externally in separate reservoirs and are circulated through the negative and positive compartments, respectively, during the operation of the battery. For the negative side of the flow battery, the primary reaction is the zinc deposition/dissolution reaction. As this takes place in a strongly acidic environment, there is always the possibility of the hydrogen evolution reaction (HER) during the zinc deposition reaction. However, the HER becomes kinetically inhibited once zinc is present on the electrode surface as the exchange current density (j_o) for HER on zinc is some seven orders of magnitude lower than it is on Pt [38]. In the charged state, the electrodeposited zinc active material is stored within the electrochemical cell on the negative electrode. At the positive electrode, the reaction here during charge is the oxidation of the Ce(III) to form Ce(IV). Due to the high standard potential of the Ce(III)/Ce(IV) couple, *viz.* 1.44 V *vs* SHE, the electron transfer reaction is inevitably accompanied to some extent by the aqueous solvent breakdown resulting in oxygen evolution at the anode. This situation is not helped by the fact that few electrode materials can withstand the high positive potential required for the cerium reaction over prolonged periods and the metal (oxide) coatings, such as the Pt|Ir on a titanium base, which currently present the most stable materials currently available for the positive electrode also tend to be good O_2 evolution catalysts. For the negative side of the flow battery, the primary reaction is the zinc deposition/dissolution reaction.

$$Zn^{2+} + 2e^- \leftrightarrow Zn_{(s)}\ E^o = -0.76\,V\ vs\ S.H.E \quad (1)$$

At the positive electrode of the zinc-cerium flow battery, the primary reaction during charge is the oxidation of the Ce(III) to form Ce(IV).

$$2Ce^{3+} \leftrightarrow 2Ce^{4+} + e^-\ E^o = 1.44\,V\ vs\ S.H.E \quad (2)$$

The overall reaction of the zinc-cerium flow cell during discharge is:

$$Zn + 2Ce(CH_3SO_3)_4 \rightarrow Zn(CH_3SO_3H)_2 + 2Ce(CH_3SO_3)_3$$
$$E^o = 2.20\,V \quad (3)$$

This indicates that during the charge process where Zn is electrodeposited at the negative electrode and Ce^{3+} is oxidised to Ce^{4+} at the positive one, there must also be movement of protons through the cation-exchange membrane, from the cerium electrolyte to the zinc electrolyte, in order to maintain charge neutrality. This, along with the increased solubility of cerium in MSA, explains the highly acidic medium used in this system. In this study, the impact of current density on the morphology of the zinc deposits was first examined using the Hull cell [39–41] arrangement. The information obtained was then applied to the redox flow cell where the impact of electrolyte flow velocity into the cell on the coulombic and cell potential efficiencies was investigated.

In general, zinc-based systems suffer from a high rate of self-discharge, *i.e* corrosion of the zinc in the electrolyte as well as that of dendritic growth, which can lead to internal short circuits and premature failures as has been found in the zinc-halogen redox flow battery [42,43]. As a result, extensive work has been carried out in order to optimize the design of electrolyte channels so as to minimize dendrite formation [44]. In the zinc-halogen batteries some of the factors that affect the zinc deposition here are the electrode substrate, the charging method, the cell geometry, the electrolyte hydrodynamics, the electrolyte composition and the zinc electrode morphology [45]. The investigation of aqueous zinc in sulfuric acid was carried out by Guillame [46] who reported that HER on stainless steel is inhibited by deposition of zinc and that the current density had little impact on the deposit morphology. The same study also reported that increasing the concentration of the zinc species (>2×10^{-1} mol dm^{-3}) yielded higher deposition current efficiencies, *viz.* 80%. In the zinc-bromine battery, HER leads to lower coulombic efficiencies and then to the non-uniform deposition of zinc on cycling [47]. Van Parys *et al.* [45] also found that the micro stirring arising from gas bubbles formed in the mass transport controlled region for the zinc electrodeposition process increased the current density as well as the pH, due to the H^+ consumption, in the immediate vicinity of the electrode surface. On the other hand, if the deposition current was in the kinetically controlled region, the current density decreased due to the increased resistance of the electrolyte. In the zinc-nickel cell, zinc dendrite penetration of the separator and redistribution of the zinc electrode active material occurred on cycling as well as a densification of the zinc electrode [47]. Ito *et al.* [48] also reported an improved cycle life of the battery at 100% depth of discharge at high electrolyte flow velocities >15 cm s^{-1}.

In the electrodeposition of metals, additives are widely used to control the form and nature of the electrodeposit (*viz.* deposit brightness, grain size, dendrites and nodules). Another objective of the additives is to reduce the HER during the zinc electrodeposition. Examples here are glue and arabic gum which are the most commonly used additives in industry for the zinc electrowinning process [49,50]. However, in this particular study, additives were not employed since the MSA electrolyte also served to suppress the formation of dendrites and the particular focus was to examine the direct impact of current density on morphology in both the Hull cell and flow cell experiments.

2. Experimental

The flow battery experiments were carried out using the system and apparatus described in reference [31]. The cell was constructed from HDPE with dimensions of 190 mm × 265 mm. Flow channels were designed into the cell to direct the flow over the electrodes. The exposed geometric areas of both positive and negative working electrodes were 10 cm × 10 cm. A 117 Nafion® membrane was used as a separator between the anode and cathode compartment in the cell (thickness = 175 μm, Dupont®) [51]. Membrane-electrode spacings were adjusted through the use of silicone rubber gaskets to yield a cell gap of ≈1 cm, giving a hydraulic diameters of the order of 1.8 cm. A peristaltic pump (Masterflex®) was employed to flow the solutions into and out of the flow cell with the aid of Masterflex® precision tubing. Typical Reynolds numbers achieved with the flow cell were in the range 25 to 172. Two 500 mL amber packer jars (FisherBrand) with a Teflon face lined cap were used as reservoirs for the flow cell. These were placed in a thermostated water bath with the operating temperature controlled by a Gallenkamp thermostirrer 95. All solutions were prepared using Milli-Q deionised water (resistivity 18.2 MΩ cm) methanesulfonic acid (70%, BASF), ZnO (99.5%, Fisher Chemicals) and cerium (III) carbonate (Sigma Aldrich or Zibo Jiahua Advanced Material Resources Co. Ltd.). The carbon composite materials used on the negative side of the flow cell were either the fluor-polymer based BMA5 or the phenolic resin based BPP4 or the polypropylene based PPG86 carbon composite electrodes, described previously [52]. They were mounted onto a titanium base plate using silver conductive paint (RS 186-3600) and araldite (Loctite 3430 A + B, Hysol®) was used to seal the mounted electrode and expose only the desired surface area. For the positive side, a 10 cm × 10 cm platinised titanium mesh (10 g m^{-2} Pt) was employed. The charge/discharge cycles were carried out using either an EG & G M100A Potentiostat/Galvanostat controlled by custom written software in LabVIEW or a Bio-Logic SP-150 potentiostat/galvanostat with a VMP3B-10 10 A current booster running EC-Lab® software. The Hull cell employed (Fig. 1 and inset) was constructed from polyvinyl carbonate and the counter electrode employed was a platinised titanium mesh, same as that used in the flow cell. The angle between the electrodes means that on application of a constant current between the electrodes, the cathode experiences a range of current densities all along its surface. The carbon composites were cleaned in methanol and dried in an argon stream prior to insertion in the Hull cell at the predefined angle. The plating solution, comprising 2.5 mol dm^{-3} Zn^{2+} in 1.5 mol dm^{-3} MSA was heated in a water bath to the desired temperature of 40 °C before being placed in the Hull cell. By applying a set current of 2 A, the current densities available for the zinc deposition process ranged from 1 mA cm^{-2} to 100 mA cm^{-2} [39–41] and this also served to maintain the temperature to within 41 ± 1 °C in the cell during the 10 min of electroplating.

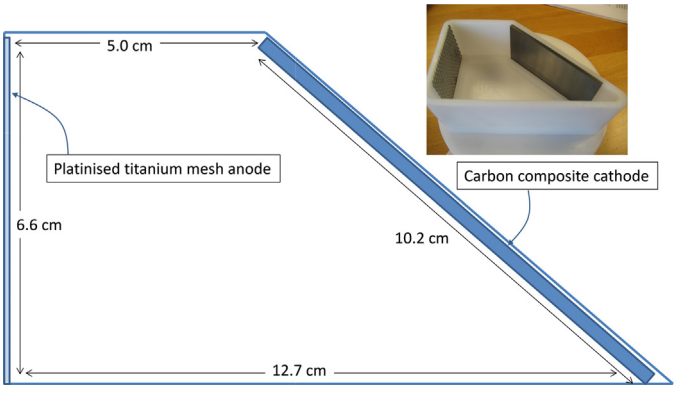

Fig. 1. Dimensions and photograph (inset) of the Hull Cell employed in the electrodeposition investigations.

3. Results and Discussion

The impact of current density on the morphology of the Zn deposit was first examined using the Hull cell. Previous work [30,31] has shown that using charge and discharge current densities lower than 25 mA cm^{-2} at a temperature of 60 °C led to a sharp fall in the coulombic efficiency of the zinc deposition/dissolution process, from ~96% down to ~81% for a 10 min charge (charge/discharge current density = 10 mA cm^{-2}). The conventional Hull cell, with no flow, was thus used to explore if this fall was caused by the different nature of zinc deposits formed at these different densities. The limitations of using such a design though have been highlighted by Low *et al.* [53] who used their rotating cylinder Hull with excellent mass transport control conditions to model the primary, secondary and tertiary current distributions associated with ohmic, kinetics and mass transport regimes in the device. Nevertheless, the much simpler design employed in our experiments did yield samples of sufficient quality to the enable key changes in morphology as a function of current density to be obtained.

The data obtained from the microscopic analysis of two of the carbon composite electrodes are shown in Figs. 2 and 3 for the BMA5 and BBP4 electrodes, respectively. The figures indicate that for current densities less than 10 mA cm^{-2}, the deposit at the end of the 10 min period is quite patchy and indeed for j < 5 mA cm^{-2}, very little zinc deposition occurred. This arises because the zinc deposition reaction is thermodynamically always the least favoured compared to HER and the current demand at these low current densities can easily be met by the latter reaction. At higher current densities, the faster kinetics of the zinc reaction takes over and zinc deposition on the carbon composite substrate occurs and its presence further inhibits the HER. What is encouraging from the microscope pictures is that over the current density range 15 mA cm^{-2} to ~60 mA cm^{-2}, the deposits obtained were relatively smooth with no evidence of dendritic growth. It is worthwhile noting that this has been achieved without the presence of surface active agents. Beyond 80 mA cm^{-2}, a roughening of the surface becomes more evident on both carbon composite substrates and reflects the rapid and less uniform growth of the zinc deposits under these conditions on the surface of the carbon substrates. It may well be that extending the electrodeposition process beyond the 10 min period chosen here could exacerbate the surface morphology of the deposits at the higher current densities, even leading to loss of deposited material under the flow conditions that would exist in the flow cell and so reduce the coulombic efficiency. However, the data obtained in this and previous work [27,28,30,31] does not indicate this to be a serious issue, possibly because of the low Reynolds numbers achieved in the flow cell. The 10 min electrodeposition period chosen was adequate to obtain a uniform zinc coating on the carbon substrates.

Typical charge/discharge curves obtained from the zinc-cerium redox flow battery at a current density of 10 mA cm^{-2} employing the BMA5 electrode are shown in Fig. 4. Charging here was carried out for 2 h from anolytes and catholytes at a temperature of 45 °C and a mean flow velocity of 9.5 cm s^{-1} into the cell. It shows a relatively flat voltage profile for both charge and discharge. The data in Table 1 summarises the results obtained from a study of flow rate dependence of the zinc and cerium electrolytes into the flow cell, carried out at a temperature of 45 °C using the BMA5 carbon composite electrode. The volumetric flow rate here was varied so that the mean flow velocity in the cell was in the range 7.5 cm s^{-1} to 13.5 m s^{-1}, corresponding to Reynolds number of ~35 and ~80

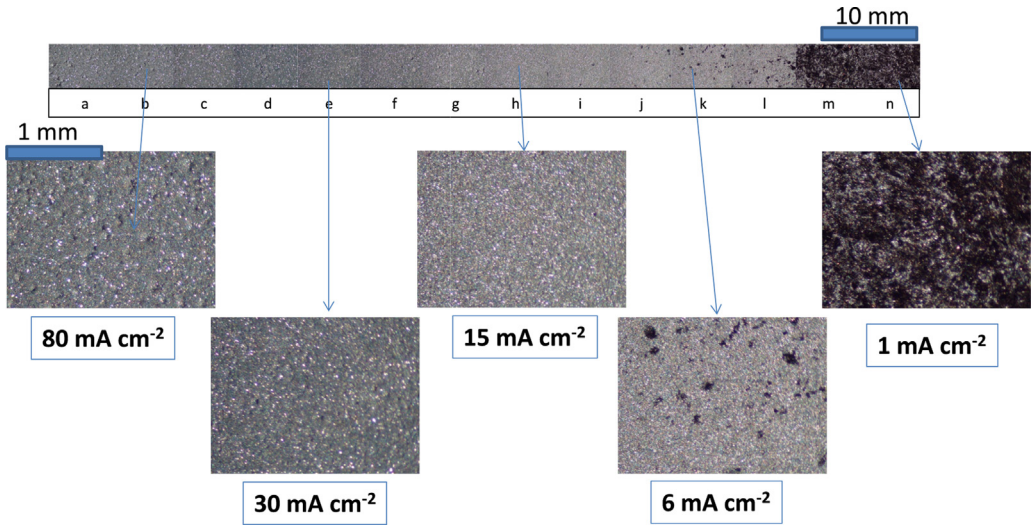

Fig. 2. Photographs of electrodeposits from Hull cell experiment using the BMA5 electrode, showing the impact of current density on the surface morphology of the zinc deposits. (Scale bars of 1 mm and 10 mm shown).

Table 1
Impact of flow velocity and charge duration on the coulombic (η_C) and cell potential (η_V) efficiencies of the Zn-Ce flow cell at 45 °C. Charge/discharge current density = 10 mA cm^{-2} on BMA5 electrode.

Mean flow velocity/cm s^{-1}	Charge duration			
	5 minutes		240 minutes	
	η_C	η_V	η_C	η_V
7.5	89%	60%	73%	60%
9	91%	61%	71%	60%
10.5	90%	59%	73%	60%
12	90%	60%	71%	59%
13.5	89%	59%	72%	60%

respectively. It is immediately obvious that flow velocity over this range has essentially no impact on the coulombic efficiency of the flow cell. What appears to be of more critical importance though is the duration of the charging process, with a coulombic efficiency of 90% obtained after a 5 min charge at a current density of 10 mA cm^{-2} but this value reduces to 72% after a four hour charge. Given that the zinc ion concentration on the negative side was 2.5 mol dm^{-3} in a solution volume of 700 cm^3 and that of the Ce^{3+} concentration in the positive side was 0.23 mol dm^{-3} (in a total cerium concentration of 0.67 mol dm^{-3}), again in a 700 cm^3 volume, it is relatively straightforward to evaluate the state of charge at the end of each of these charging periods and so, the depletion of the electroactive species. For the 5 min charge period, the reduction in the concentration of the Zn^{2+} ion concentration in the negative electrolyte is insignificant (<0.003 mol dm^{-3}) and correspondingly, that in the Ce^{3+} concentration is ~0.006 mol dm^{-3}. After the 4 h charge, the zinc concentration was reduced to 2.39 mol dm^{-3}, representing still only a 4% state of charge. However, for the Ce^{3+} concentration, this has dropped to 0.017 mol dm^{-3}, representing a 93% state of charge. If we take the mass transport coefficient k_m in the cell to be 5.0×10^{-3} cm s^{-1} [32], we can estimate the mass transport limiting current for the Ce^{3+} oxidation at the positive electrode at that point to be ~0.8 A, below the charging current used for this study. It was inevitable therefore that coulombic efficiency would be significantly lowered here since the current would also have been involved in oxygen evolution at the anode and this was evident from the presence of gas bubbles in the flow tubes. Hence, this will always occur at long charge times at the current of 1 A

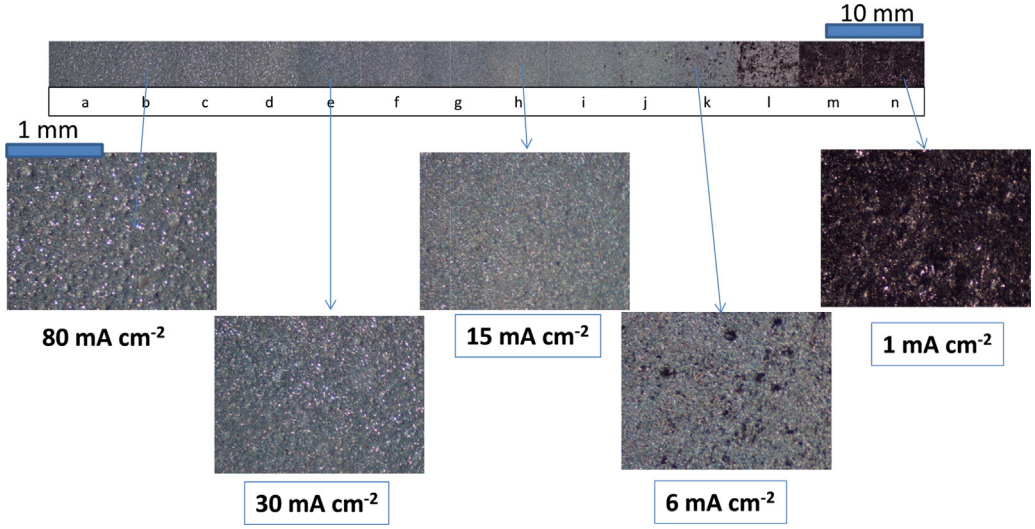

Fig. 3. Photographs of electrodeposits from Hull cell experiment using the BPP4 electrode, showing the impact of current density on the surface morphology of the zinc deposits. (Scale bars of 1 mm and 10 mm shown).

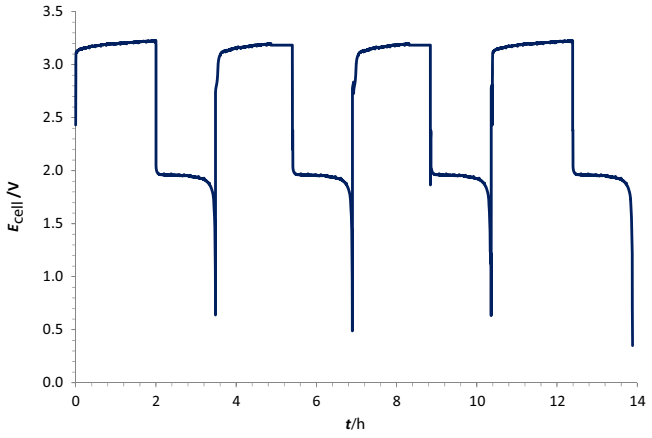

Fig. 4. Charge/discharge cycles for the Zn-Ce RFB at an electrolyte temperature of 45 °C and mean flow velocity of 9.0 cm s^{-1}. 2 hour charge at a current density of 10 mA cm^{-2}. BMA5 electrode.

when the concentration of the limiting reactant here, which is the Ce^{3+} species, approaches 0.02 mol dm^{-3}. It is worth noting that the cell potential efficiency remains invariant with charging time indicating that at the very least, the ohmic resistance was not altered by this depletion. This is not unexpected as the acid concentration was 3.5 mol dm^{-3} and any oxygen bubbles produced at the electrode surface, which could also contribute to ohmic losses, would have been removed by the flowing solution. Nevertheless, the cell potential efficiency values here are not high and as has been noted previously [31], this has been attributed to the large area resistance (~51 Ω cm^2) arising from the mounting of the carbon composites onto the support plate in the cell. Measures are currently in hand to decrease this value by *ca.* two orders of magnitude in order to increase the dc roundtrip energy efficiency of the charge/discharge cycles at the high current used in this flow cell system. This high area resistance therefore severely limited the magnitude of the discharge current density that could be applied to the flow cell as the cut-off voltage during the measurements was set to 0.5 V.

Fig. 5 again shows the charge/discharge data obtained from the flow cell operated at 45 °C with the BPP4 carbon-composite electrode. In this figure however, it can be seen that although the discharge current employed was always set to 10 mA cm^{-2}, the charging current was varied from 1 A to 4 A (10 mA cm^{-2} to 40 mA cm^{-2}). As expected, the cell voltage during the 30 min charge increased with the charging current employed, from 3.04 V at 1 A to

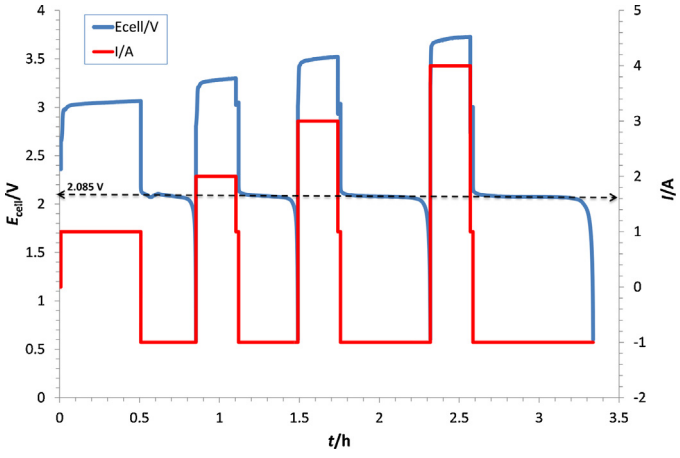

Fig. 5. Charge/discharge data for the Zn-Ce RFB at 45 °C and mean flow velocity of 10 cm s^{-1}. Charging current ranged from 10 mA cm^{-2} to 40 mA cm^{-2} for 10 min. Discharge current was 10 mA cm^{-2}. BPP4 electrode.

Table 2
Impact of charging current density on the coulombic (η_C) and cell potential (η_V) efficiencies of the Zn-Ce flow cell at 45 °C, using the PPG86 carbon composite electrode. Mean flow velocity = 7.5 cm s^{-1}.

j_{charge} /mA cm^{-2}	$j_{discharge}$ /mA cm^{-2}	Charge time /s	η_C	η_V
10	10	1800	89%	60%
30	10	1800	91%	68%
40	10	1800	91%	69%
50	10	1800	90%	69%

3.72 V at 4 A. However, the discharge voltage remained remarkably constant at 2.085 V, regardless of the charging current used. This signifies therefore that from an electrochemical viewpoint, the zinc deposits at these different voltages exhibit very similar behaviour with regards to electrical resistance and dissolution rates in the MSA medium.

The data obtained from a similar study using the PPG86 carbon-composite electrode is summarized in Table 2 and this shows that the coulombic efficiency is again not affected by the different charging current densities employed here, with values of 90 ±1% being obtained. It is worth noting though that the cell potential efficiencies shown in the table were determined at the current density of 10 mA cm^{-2}. This was done for each of the higher charging current used by reducing the current to 1 A for 30 s at the end of the charging period. What the data in the Table 2 indicates is that there is an improvement of ~10% in the cell potential efficiency measured from the deposits achieved using current densities higher than 10 mA cm^{-2}. This suggests that the surface morphology of the deposits at the higher current density presents an improved surface for more efficient zinc deposition at the lower currents. It reinforces the Hull Cell data which indicated that at current densities lower than 15 mA cm^{-2}, (1.5 A for the flow cell), there was always the probability of areas on the surface where there would be a negligible or low amounts of zinc deposition onto the carbon composite surface. In these areas, the HER would dominate on the carbon composite surface and the production of even small amounts of H_2 bubbles on the surface would tend to block zinc deposition and increase local electrical resistance. The surface deposit then would also tend to be patchy. At the higher current densities however, more uniform zinc coatings were obtained and further deposition on these surfaces, even at the lower current densities would not lead to the HER on the zinc surface since the latter reaction, as has been previously noted, is strongly inhibited here. Thus, high coulombic efficiencies could be maintained in these instances even at low charging current densities.

4. Conclusions

An examination of the parameters that could influence the performance of the zinc-cerium redox flow has been carried out. Although the flow rate, albeit over the narrow range explored, did not have a particular strong effect on performance, the current density employed for the deposition reaction determined the uniformity and morphology of the zinc deposits formed, with current densities greater than 10 mA cm^{-2} recommended for this process. Depletion of the electroactive species was not a problem for the zinc under the operational conditions employed in the study, but for the Ce(III) species (~0.4 M), charging periods greater than ~3 h presented a significant issue due to a depletion of the species leading to a reduction in the current efficiency caused by secondary oxygen evolution reaction. The data also revealed that lower charging currents could be employed without any loss in coulombic efficiency once a complete zinc layer was present on the carbon composite surface. In this way, high states of charge could be reached in the system without reduction in the energy efficiency.

Care has to be taken however to ensure that the depletion of the cerium electroactive species does not occur at the long charging times, which would inevitably result in a loss in current efficiency.

References

[1] U.S. Dept. of Energy, National Aeronautics and Space Administration., NASA TM-79067 (1979) 1-53.
[2] P.C. Butler, P.A. Eidler, P.G. Grimes, S.E. Klassen, R.C. Miles, in: D. Linden, T.B. Reddy (Eds.), Handbook of Batteries, 3rd edn, McGraw-Hill, 2002, p. 39.
[3] T. Shigematsu, SEI Technical Rev. 73 (2011) 5–13.
[4] C. Liu, R. Galasco, R. Savinell, Enhancing Performance of the Ti(III)/Ti(IV) Couple for Redox Battery Applications, J. Electrochem. Soc. 128 (1981) 1755–1757.
[5] R. Savinell, C. Liu, R. Galasco, S. Chiang, J. Coetzee, Discharge Characteristics of Soluble Iron-Titanium Battery System, J. Electrochem. Soc. 126 (1979) 357–360.
[6] Y. Matsuda, K. Tanaka, M. Okada, Y. Takasu, M. Morita, M. Matsumura-Inoue, A rechargeable redox battery utilizing ruthenium complexes with non-aqueous organic electrolyte, J. Appl. Electrochem. 18 (1988) 909–914.
[7] M. Skyllas-Kazacos, M. Rychcik, R. Robins, A. Fane, M. Green, New All-Vanadium redox flow cell, J. Electrochem. Soc. 133 (1986) 1057.
[8] M. Skyllas-Kazacos, F. Grossmith, Efficient Vanadium Flow Cell, J. Electrochem. Soc. 134 (12) (1987) 2950–2953.
[9] B. Fang, S. Iwasa, Y. Wei, T. Arai, M. Kumagai, A study of the Ce(III)/Ce(IV) redox couple for redox flow battery application, Electrochim. Acta 47 (2002) 3971–3976.
[10] F.Q. Xue, Y.L. Wang, W.H. Wang, X.D. Wang, Investigation on the electrode process of the Mn(II)/Mn(III) couple in redox flow battery, Electrochim. Acta 53 (2008) 6636–6642.
[11] M. Skyllas-Kazacos, Novel vanadium chloride/polyhalide redox flow battery, J. Power Sources 124 (2003) 299–302.
[12] H. Tao, X. Fangqin, Investigation on manganese (Mn2+/Mn3+)-vanadium (V2+/V3+) redox flow battery, Power and Energy Engineering Conference, (2009) APPEEC 2009 Asia-Pacific.
[13] Q. Liu, A. Sleightholme, A. Shinkle, Y. Li, L. Thompson, Non-aqueous vanadium acetylacetonate electrolyte for redox flow batteries, Electrochem. Commun. 11 (2009) 2312–2315.
[14] D. Pletcher, R. Wills, A novel flow battery: A lead acid battery based on an electrolyte with soluble lead(II). Part IV: the influence of additives, J. Power Sources 149 (2005) 96–102.
[15] D. Pletcher, H.T. Xhou, G. Kear, C.T.J. Low, F.C. Walsh, R.G.A. Wills, A novel flow battery: A lead acid battery based on an electrolyte with soluble lead(II). Part V: Studies of the lead negative electrode, J. Power Sources 180 (2008) 621–629.
[16] Y. Xu, Y.H. Wen, J. Cheng, G.P. Cao, Y.S. Yang, Study on a single flow acid Cd-chloranil battery, Electrochem. Commun. 11 (2009) 1422–1424.
[17] D. Scamman, G. Reade, E. Roberts, Numerical modelling of a bromide–polysulphide redox flow battery. Part 1: Modeling approach and validation for a pilot-scale system, J. Power Sources 189 (2009) 1220–1230.
[18] J.Q. Pan, Y.Z. Sun, J. Cheng, Y.H. Wen, Y.S. Yang, P.Y. Wan, Study on a new single flow acid Cu-PbO2 battery, Electrochem. Comm 10 (2008) 1226–1229.
[19] H. Lim, A. Lackner, J. Knechtli, Zinc-bromine secondary battery, J. Electrochem. Soc. 124 (1977) 1154–1157.
[20] D. Linden, Handbook of Batteries and Fuel Cells, 2nd Edition, McGraw-Hill, New York, 1995, pp. 37.
[21] L. Zhang, J. Cheng, Y. Yang, Y. Wen, X. Wang, G. Cao, Study of zinc electrodes for single flow zinc/nickel battery application, J. Power Sources 179 (2008) 381–387.
[22] J. Jorné, J.T. Kim, D. Kralik, The zinc-chlorine battery: half-cell overpotential measurements, J. Appl. Electrochem. 9 (1979) 573–579.
[23] Y. Wen, J. Cheng, S. Ning, Y. Yang, Preliminary study on zinc-air battery using regeneration electrolysis with propanol oxidation as a counter electrode reaction, J. Power Sources 188 (2009) 301–307.
[24] P.K. Leung, X. Li, C. Ponce de Leon, L. Berlouis, C.T.J. Low, F.C. Walsh, Progress in flow batteries, remaining challenges and their applications on energy conversion and storage, RSC Advances 2 (27) (2012) 10125–10156.
[25] R.L. Clarke, B.J. Dougherty, S. Harrison, J.P. Millington, S. Mohanta, US Patent Application 2004/0202925 A1, (2004).
[26] R.L. Clarke, B.J. Dougherty, S. Harrison, J.P. Millington, S. Mohanta, US Patent Application 2006/0063065 A1, (2005).
[27] P.K. Leung, C. Ponce de Leon, C.T.J. Low, A.A. Shah, F.C. Walsh, Characterization of a zinc-cerium flow battery, J. Power Sources 11 (2011) 5174–5185.
[28] P.K. Leung, C. Ponce-de-León, C.T.J. Low, F.C. Walsh, Zinc deposition and dissolution in methanesulfonic acid onto a carbon composite electrode as the negative electrode reactions in a hybrid redox flow battery, Electrochim. Acta 56 (2011) 6536–6546.
[29] P.K. Leung, C. Ponce de León, F.C. Walsh, An undivided zinc–cerium redox flow battery operating at room temperature (295 K), Electrochem. Commun. 13 (8) (2011) 770–773.
[30] G. Nikiforidis, L. Berlouis, D. Hall, D. Hodgson, Impact of electrolyte composition on the performance of the zinc-cerium redox flow battery system, J. Power Sources 243 (2013) 691–698.
[31] G. Nikiforidis, L. Berlouis, D. Hall, D. Hodgson, Evaluation of carbon composite materials for the negative electrode in the zinc-cerium redox flow cell, J. Power Sources 206 (2012) 497–503.
[32] G. Nikiforidis, L. Berlouis, D. Hall, D. Hodgson, An electrochemical study on the positive electrode side of the zinc-cerium hybrid redox flow battery, Electrochim. Acta 115 (2014) 621–629.
[33] G. Nikifordis, L. Berlouis, D. Hall, D. Hodgson, A study of different carbon composite materials for the negative half-cell reaction of the zinc cerium hybrid redox flow cell, Electrochim. Acta 113 (2013) 412–423.
[34] T. Raju, C.A. Basha, Process parameters and kinetics for the electrochemical generation of Cerium(IV) methanesulphonate from Cerium(III) methanesulphonate, J. Ind. Eng. Chem. Res. 47 (2008) 8947–8952.
[35] J. Ludek, W. Yuezhou, M. Kumagai, Electroxidation of Concentrated Ce(III) at Carbon Felt Anode in Nitric Acid Media, J. Rare Earths 24 (2006) 257–263.
[36] Z. Xie, D. Zhou, F. Xiong, S. Zhang, K. Huang, Cerium-zinc redox flow battery: Positive half-cell electrolyte studies, J. Rare Earths 29 (6) (2011) 567.
[37] F.C. Walsh, C. Ponce de Léon, L., Berlouis, G., Nikiforidis, L.F. Arenas-Martínez, D., Hodgson, D. Hall, The development of Zn-Ce hybrid redox flow batteries for energy storage and their continuing challenges, submitted manuscript to ChemPlusChem: Special Issue–Metal-Air and Redox Flow Batteries.
[38] D. Pletcher, F.C. Walsh, Industrial Electrochemistry, Blackie Academic and Professional, London, 1993.
[39] M. Matlosz, C. Creton, C. Clerc, D. Landolt, Secondary Current Distribution in a Hull Cell - Boundary Element and Finite Element Simulation and Experimental Verification, J. Electrochem. Soc. 134 (1987) 3015–3021.
[40] A.C. West, M. Matlosz, D. Landolt, Primary current distribution in the Hull cell and related trapezoidal geometries, J. Appl. Electrochem. 22 (1992) 301–303.
[41] http://www.schloetter.co.uk/plating-equipment/Hull-cells-and-plating-test-equipment.htm, accessed 9th December 2013.
[42] G. Brodt, J., Haas, W., Hesse, H.U. Jaqer, Method for electrolytic galvanizing. using electrolytes containing alkane sulfonic acid, US Patent 2003/0141195 Al.(31/07/2003).
[43] A.J. Bard, L.R. Faulkner, Electrochemical Methods: Fundamentals and Applications, John Wiley & Sons, New York, 1980, pp. 291–298, 539-540.
[44] C. Ponce de Leon, A. Frias-Ferrer, J. Gonsalez-Garcia, D.A. Szanto, F.C. Walsh, Redox flow cells for energy conversion, J. Power Sources 160 (2006) 716–732.
[45] H. Van Parys, G. Telias, V. Nedashkivskyi, B. Mollay, I. Vandendael, S. Van Damme, J. Deconinck, A. Hubin, On the modelling of electrochemical systems with simultaneous gas evolution. Case study: The zinc deposition mechanism, Electrochim. Acta 55 (2010) 5709–5718.
[46] P. Guillaume, N. Leclerc, C. Boulanger, J. Lecuire, F. Lapicque, Investigation of optimal conditions for zinc electrowinning from aqueous sulfuric acid electrolytes, J. Appl. Electrochem 37 (11) (2007) 1237–1243.
[47] J. McBreen, Rechargeable zinc batteries, J. Electroanal. Chem. 168 (1-2) (1984) 415–432.
[48] Y. Ito, M. Nyce, R. Plivelich, M. Klein, D. Steingart, S. Banerjee, Zinc morphology in zinc-nickel flow assisted batteries and impact on performance, J. Power Sources. 196 (2011) 2340.
[49] D.J. MacKinnon, R.M. Morrison, J.E. Mouland, P.E. Warren, The effect of glue and antimony on zinc electrowinning from Kidd Creek electrolyte, J. Appl. Electrochem. 20 (1990) 728–736.
[50] C. Tripathy, S.C. Das, P. Singh, G.T. Hefter, V.N. Mistra, Zinc electrowinning from acidic sulphate solutions Part IV: effects of perfluorocarboxylic acids, J. Electroanal. Chem. 565 (2004) 49–56.
[51] Z.Q. Mao, Fuel Cell, Chemical Industry Press 63 (2005) 33–47.
[52] http://www.eisenhuth.de/pdf/SIGRACET_Datenblaetter.pdf, accessed 9th December 2013.
[53] C.T.J. Low, E.P.L. Roberts, F.C. Walsh, Numerical simulation of current, Potential and Concentration Distributions along a rotating cyclinder Hull cell Cathode, Electrochim. Acta 52 (2007) 3831–3840.